Covalent Nanoparticle Assembly onto Random Copolymer Films

Marla D. McConnell, Shu Yang,* and Russell J. Composto*

Department of Materials Science and Engineering and Laboratory for Research on the Structure of Matter, University of Pennsylvania, Philadelphia, Pennsylvania 19104

Received October 14, 2008; Revised Manuscript Received November 19, 2008

ABSTRACT: We present a novel class of nanoparticle-decorated surfaces: amine-functionalized silica nanoparticles covalently attached to poly(styrene-*random*-acrylic acid) films and carboxylic acid-terminated self-assembled monolayers (SAMs). The dependence of the particle attachment kinetics on the concentration of particles in solution and acrylic acid moieties in the polymer backbone was investigated and was compared to the observed kinetics with SAM substrates. The kinetics on the polymer films included three distinct stages, which were governed by the acrylic acid concentration-dependent morphological changes of the films under the reaction conditions. The first stage was an induction period with little change in the particle coverage with time, followed by a rapid rise in the coverage, and finally a plateau. The maximum coverage achieved for the polymer films, 70%, was nearly twice that of the SAM substrates, which followed diffusion-limited coverage kinetics prior to reaching saturation. This enhanced coverage is attributed to the swelling of the acrylic acid groups at the film surface in the reaction solvent, which increases the surface area and roughness of the substrate. This approach is a reproducible way of preparing nanoparticle-decorated, chemically robust surfaces with controlled coverages and have potential applications for controlling surface wettability, optical properties, and cellular adhesion.

Introduction

Nanoparticle-decorated surfaces allow for precise control of physical and chemical surface functionality and are being investigated in many research fields in which tunable surface properties are required.[1] Specifically, by varying the chemical nature of the particles (polymeric, metallic, or semiconducting), their size, number density, spacing, clustering, and attachment chemistry, it is possible to manipulate the chemical and physical properties (i.e., wettability,[2−5] electrical conductivity,[6,7] and optical activity[8−11]) of the composite surface. These modified surfaces have been used in applications including magnetic storage,[12,13] photocurrent generation,[14] catalysis,[15,16] and cell adhesion.[17,18]

The assembly and structure of nanoparticle arrays are governed by the underlying variables involved in the nanoparticle−substrate interactions, including the structure and chemical composition of the substrate and the surface functionality of the particles. There have been many techniques developed to control the assembly of nanoparticles on nonpolymeric surfaces. Electrostatic interactions have been successfully used to produce complex nanoparticle assemblies, such as particle concentration gradients[19,20] and multilayered structures.[21−23] Additionally, submonolayers of particles on surfaces have been achieved by the use of gold ion micellization[24,25] and gold nanoparticle−thiol bonding.[26]

The use of polymeric substrates in controlling nanoparticles at a surface is of particular interest because polymer structure and functionality can be readily manipulated via various synthetic routes. To date, studies using polymeric substrates have employed block copolymers,[27−29] statistical copolymers,[30] semicrystalline polymers,[31] and tethered polymer chains.[32] Many attachment methods, including hydrogen bonding,[28,30] gold−thiol bonding,[31] and electrostatic interactions,[32−34] have been used to assemble nanoparticles at polymer surfaces. Because these methods do not produce a strong covalent linkage between the particles and the substrates, the stability of these systems over a wide range of environmental conditions (i.e., solvent, temperature, ion concentration, etc.) is restricted, which in turn limits their applicability. Additionally, the kinetics of particle attachment to these polymer substrates have not been studied. To prepare environmentally robust, reproducible polymer−nanoparticle systems, their reaction kinetics must be well-understood.

Herein, we develop a new synthetic strategy to covalently attach amine-modified silica nanoparticles onto the acrylic acid moieties in poly(styrene-*random*-acrylic acid), P(S-*ran*-AA), films and carboxylic acid-terminated self-assembled monolayers (SAMs) on silicon substrates. Random copolymers were chosen to provide a surface with both reactive sites (i.e., acrylic acid) and solvent stability (i.e., styrene). These materials offer an advantage over previous nanoparticle surfaces because the covalent linkage is stable over a wide range of environmental conditions. By varying the mole fraction of acrylic acid in the copolymer, nanoparticle concentration in suspension, and the reaction time, the coverage and spacing of the particles could be controlled in a reproducible manner. The nanoparticle coverage kinetics exhibit three distinct regions: an induction period in which the coverage increases very little with time, a period in which the coverage increases dramatically with time, and a saturation region. These kinetic regions originate from the structural rearrangement of the film surfaces under the reaction conditions, which was followed by in-situ AFM. The induction period was attributed to the initial lateral confinement of the acrylic acid groups at the surface of the film. Surface acrylic acid swelling mobilized the polymer chains for efficient reaction toward the nanoparticles, leading to a rapid increase in coverage and the end of the induction period. During the saturation phase of the kinetics, the maximum coverage was governed by the equilibrium surface morphology of the films and the number of available particles (at low particle concentrations). The highest surface coverage attained on the P(S-*ran*-AA) copolymers was around 70%, corresponding to a full close-packed monolayer of particles. On the SAMs, the maximum surface coverage of nanoparticles was around 30−35% and the adsorption kinetics had a $t^{1/2}$ dependence before reaching saturation. These kinetics were observed because, unlike the polymer substrates, the SAM surfaces did not undergo any swelling under the reaction conditions. This work is novel in two respects: it is the first example of strong covalent nanoparticle attachment to polymer substrates and the first use of

* Corresponding authors. E-mail: shuyang@seas.upenn.edu (S.Y.); composto@seas.upenn.edu (R.J.C.).

10.1021/ma8023156 CCC: $40.75
Published on Web 12/19/2008

in-situ AFM to study substrate effects on nanoparticle coverage kinetics. These nanoparticle decorated polymer surfaces provide a unique platform for investigating the effect of nanoscale roughness on surface wettability.

Experimental Section

Materials. Dimethyl sulfoxide (DMSO) (anhydrous, 99.9+%), ethanol (200 proof), (3-aminopropyl)triethoxysilane (APTES) (99%), 1-ethyl-3-(3-(dimethylamino)propyl)carbodiimide hydrochloride (EDC) (≥98.0%), *N*-hydroxysuccinimide (NHS) (98%), and *N,N*-dimethylformamide (DMF) (≥99.9%) were purchased from Aldrich and used as received. Methanol (HPLC grade), toluene (HPLC grade), and water (DIUF) were purchased from Fisher Scientific and used as received. Triethoxysilylpropylsuccinic anhydride (TESPA) (95%) was purchased from Gelest, Inc., and used as received. 2,2′-Azobis(isobutyronitrile) (AIBN) (Aldrich, 98%) was recrystallized from cold methanol prior to use. Styrene (S) (Aldrich, 99%) and *tert*-butyl acrylate (*t*BA) (Alfa Aesar) were passed through a column filled with basic alumina (Aldrich) before use.

Nanoparticle Modification. Silica nanoparticles, 15 ± 3.5 nm in diameter (Nissan Chemical, 30 wt % in isopropanol), were pelletized by centrifugation at 11 000 rpm for 3 h. The solvent was then exchanged to anhydrous DMSO, and the suspension was sonicated for at least 15 min to redisperse the particles. The pelletization/solvent exchange procedure was repeated two more times. The particles were then amine functionalized via reaction with aminopropyltriethoxysilane (APTES). An excess of 5% (v/v) solution of APTES was added to the nanoparticle suspension in anhydrous DMSO and allowed to react for 8 h. The nanoparticles were then purified via centrifugation using the same procedure as above and solvent exchanged into ethanol.

RAFT Polymerization of Poly(styrene-*random*-*tert*-butyl acrylate), P(S-*ran*-tBA). In a typical synthesis, a 50 mL Schlenk flask was charged with *t*BA (6.6 mL, 45 mmol), styrene (15.5 mL, 135 mmol), and 8 mL of benzene. The flask was sealed and subjected to three freeze−pump−thaw cycles to degas the polymerization solution. AIBN (0.0084 g, 0.051 mmol) and cyanomethyldodecyltrithiocarbonate (generously provided by Prof. Bradford Wayland) (0.033 g, 0.125 mmol) were added to the frozen reaction mixture under a nitrogen flush. The flask was then sealed and placed in a thermostated oil bath at 60 °C and allowed to react for 24 h. The resulting polymer was purified by crystallization in cold MeOH and then dried under vacuum at room temperature. The chemical composition of the resulting polymers were calculated using ^{1}HNMR (Bruker DMX-300 MHz spectrometer) (δ, ppm in $CDCl_3$): 1.20−2.20 (m, 5H, CH_2CH of PS, CH_2CH of P*t*BA), 1.50 (s, 9H, $C(CH_3)_3$ of P*t*BA), 2.22 (s, 1H, CH_2CH of P*t*BA), 6.30−7.30 (m, 5H, C_6H_5 of PS).

Two P(S-*ran*-*t*BA*)* were prepared having similar molecular weights but different molar concentrations of functional units, *t*BA. The normalized molar ratio for R30 was PS:P*t*BA 70:30 (feed ratio: 75:25) and for R50 was PS:P*t*BA 53:47 (feed ratio: 50:50). The molecular weight and polydispersity of the copolymers were characterized with GPC (PL-GPC50, Polymer Laboratories). The GPC was equipped with a PL MIDAS830 autosampler, PLgel 5 L MIXEDC columns, and a PL COM9 refractive index detector against linear polystyrene standards in THF (1 mL min^{-1}) at 27 °C. The M_n of R30 and R50 were 56 000 and 42 000, respectively, with polydispersities of 1.27 and 1.32. Differential scanning calorimetry (2920 DSC, TA Instruments) was performed on the polymers at a heating rate of 10 °C/min. Glass transition temperatures were measured from the third heating cycle to be 86.0 ± 0.6 and 76.7 ± 0.6 °C for the R30 and R50 polymers, respectively. The existence of a single glass transition for each polymer is consistent with a random distribution of *t*BA groups, and the values were those expected, given the respective molar fractions of styrene and *t*BA along the backbone.

Substrate Preparation. Silicon substrates were immersed in piranha solution (3:7 v:v H_2O_2:H_2SO_4) at 80 °C for 20 min. The substrates were subsequently washed with DIUF water, dried in nitrogen, and exposed to UV ozone (UVO-Cleaner Model 42, Jelight Co. Inc.) for 10 min to form a uniform oxide layer. For the SAM substrates, an anhydride-terminated self-assembled monolayer was formed on the surface of the silicon oxide by immersing the silicon wafers in a 5% (v/v) solution of triethoxysilylpropylsuccinic anhydride in toluene for 16 h under argon.[35,36] The substrates were then sonicated sequentially in toluene, DMF, and water. Sonication of the SAM substrates in water converted the anhydride moieties to carboxylic acid groups. The resulting SAMs had a thickness of 0.89 ± 0.2 nm, as determined by ellipsometry (Auto El, Rudolph Research), and a static contact angle of 26.5 ± 6.2° (Ramé-Hart), which is consistent with literature values.[35,36]

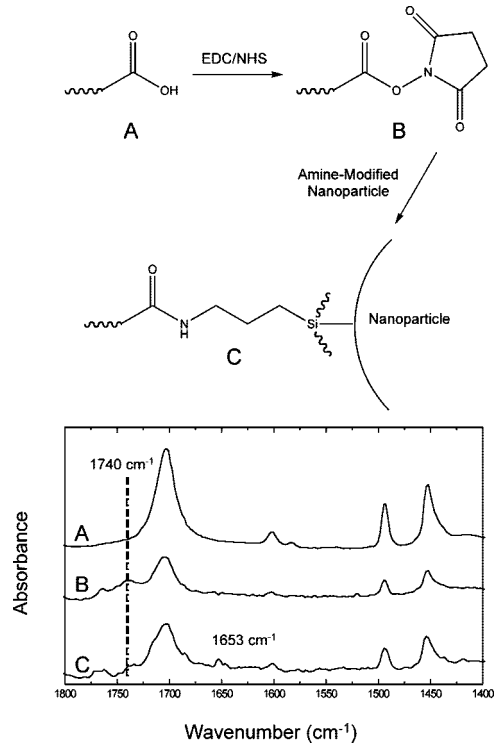

Figure 1. Reaction scheme and ATR-FTIR spectra for the covalent coupling of amine-modified nanoparticles to R50 copolymer films: (A) annealed R50 film; (B) NHS-activated R50 film; (C) amine-modified nanoparticles covalently linked to the R50 copolymer films via amide bonds, 1653 cm^{-1}.

To prepare polymer films on silicon, polymer solutions (toluene, 5 wt %) were spin-coated (2000 rpm, 60 s) onto cleaned silicon substrates to form 200 nm thick films, as determined by ellipsometry. The polymer films were dried overnight in a fume hood and then annealed at 185 °C for 15 h under argon. These annealing conditions resulted in complete deprotection of the *tert*-butyl groups, as characterized using ATR-FTIR spectroscopy (Nicolet Nexus 470 with MCT-B detector, Harrick GATR). The spectra of the as-cast polymer films show the characteristic bending and stretching modes associated with *tert*-butyl acrylate and styrene. The absorption bands originating from poly(*tert*-butyl acrylate) are located at 1730 cm^{-1} ($\nu_{C=O}$, ester), 1394/1368 cm^{-1} (ν_{CH_3}), 1277/1258 cm^{-1} (ν_{C-O-O}), and 1160 cm^{-1} (ν_{C-O}). Those bands originating from polystyrene are located between 1600 and 1400 cm^{-1} ($\nu_{C=C,aromatic}$). After annealing the R30 and R50 polymer films at 185 °C for 15 h, the peaks associated with the *tert*-butyl protecting group disappeared completely, and the carbonyl stretching mode underwent a blue shift of about 30 cm^{-1} and broadened (Figure 1A). These changes in the carbonyl peak are consistent with deprotection of the *tert*-butyl group to form acrylic acid.

Coupling Amine-Modified Nanoparticles to P(S-*ran*-AA)- and SAM-Modified Substrates. The nanoparticle attachment chemistry to P(S-*ran*-AA) films and SAMs is described in the top of Figure 1. Using submicron-sized gold particles, Plummer and Bohn applied a similar attachment chemistry on thiol-modified

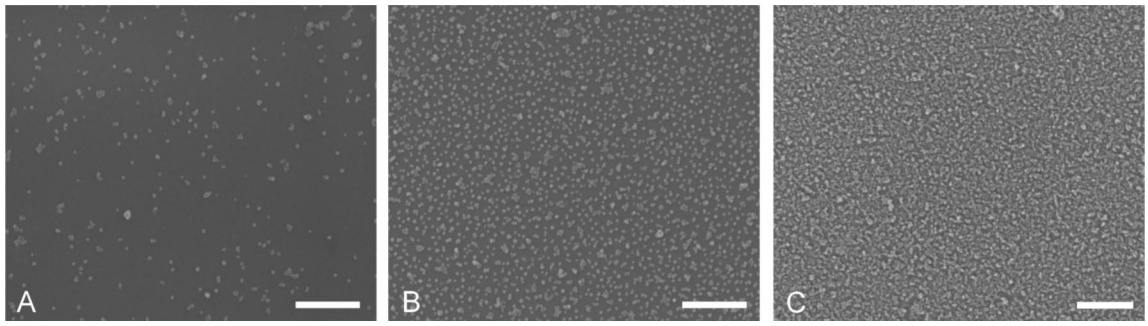

Figure 2. SEM images of the surface of nanoparticle-decorated R30 films after reaction times of (A) 15, (B) 150, and (C) 240 min. Scale bars are 500 nm.

surfaces.[37] R50 and R30 polymers were immersed in 1 M phosphate buffer (pH 8) for 2 h and then washed thoroughly with DIUF water. There are two steps in the covalent attachment of amine-modified silica nanoparticles to the acid groups in the P(S-*ran*-AA) and the SAM. In the first step, as illustrated at the top of Figure 1, the P(S-*ran*-AA) films and SAM-modified substrates were immersed in solution of EDC (0.1 M) and NHS (0.2 M) in DIUF water for 1 h, in order to activate the acrylic acid groups with the NHS. The FTIR spectrum of NHS-activated acrylic acid in the R50 polymer can be seen in Figure 1B, where the strong band at 1740 cm^{-1} is attributed to the succinimidyl carbonyl ($\nu_{C=O}$). In the second step, the activated substrates were directly immersed into 0.05, 0.01, or 0.005 wt % suspensions of amine-modified nanoparticles in ethanol for varying amounts of time (0−540 min). The substrates were immersed upside-down in the nanoparticle suspensions to prevent clusters of particles from falling onto the substrates. This geometry minimized the number of particles that nonspecifically adhered to the substrates and is responsible, in part, for the highly reproducible coverages and spacing observed in this study. Once the substrates were removed from the nanoparticle suspensions, they were immediately swirled in ethanol for 5 min, then washed vigorously with DIUF water, and dried in a stream of nitrogen. Covalent attachment of the nanoparticles by amide bond formation was confirmed by ATR-FTIR of the R50 substrate (Figure 1C) where the band at 1653 cm^{-1} is attributed to the amide carbonyl ($\nu_{C=O}$). Each set of conditions (surface type, immersion time, and nanoparticle concentration) was repeated to generate two sample sets on different days, and the reported data were obtained from both sets.

Characterization of Nanoparticle-Decorated Surfaces. The coverage of amine-modified nanoparticles coupled to the surface of the polymers and SAMs as a function of time was characterized with scanning electron microscopy (SEM, FEI Strata DB235). Percent particle coverage was measured from 10 images of nonoverlapping regions on each individual sample (20 images for each set of conditions) using ImageJ. Error bars in the percent coverage data represent one standard deviation.

Characterization of Polymer Substrate Surfaces. The surface morphology evolution of R30 and R50 polymers under the nanoparticle coupling conditions was monitored using atomic force microscopy (AFM, PicoPlus Molecular Imaging, Agilent Technologies). The tips had nominal spring constants of 48 N/m and diameters <10 nm. In-situ imaging was performed in a liquid cell, first with pH 8 phosphate buffer for 2 h, followed immediately by DIUF water (to simulate the EDC/NHS coupling step) for 1 h, and then by ethanol. Images were taken in tapping mode, with scan speeds of 0.65−0.8 Hz. Tip resonant frequencies were 190 and 75 kHz in air and solution, respectively. All reported roughness values were calculated from 1 μm^2 areas as rms roughness. The wettabilities of the polymer film surfaces under the same conditions as the in-situ AFM imaging were characterized by measuring the static contact angle (Rame-Hart). ImageJ was used to determine the resulting contact angle.

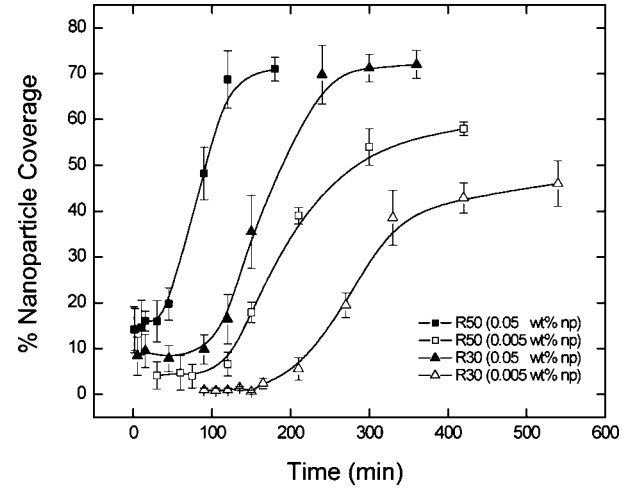

Figure 3. Percent nanoparticle coverage on the random copolymer films vs immersion time in nanoparticle solution. Particle coverage kinetics are shown as a function of polymer acrylic acid content and particle concentration: (■) R50, 0.05 wt % nanoparticles; (▲) R30, 0.05 wt % nanoparticles; (□) R50, 0.005 wt % nanoparticles; (△) R30, 0.005 wt % nanoparticles. All four sets of data display three distinct regions in the kinetic profile, an induction period, a rapid increase in the percent coverage, and a plateau region. Both the R50 and R30 polymer films reach 70% coverage at 0.05 wt % particle concentration, which corresponds to a random close-packed monolayer of particles. Note: lines are a guide to the eye.

Results and Discussion

1. Kinetics of the Nanoparticle Coupling Reaction to R30 and R50 Films. The reaction kinetics of nanoparticle coupling to the polymer films was followed by allowing the R30 and R50 polymers to react with either a 0.05 or a 0.005 wt % nanoparticle suspension for between 30 s and 540 min. The percent coverage of particles on the P(S-*ran*-AA) films was determined by quantitative analysis of SEM images. SEM images of the nanoparticle decorated R30 films can be seen in Figure 2A−C. After 15, 150, and 240 min, the particle coverage is 5, 25, and 70%, respectively. Throughout the entire reaction period, the nanoparticles remained discrete and were uniformly distributed over the surface of the film. Note that even at 70% coverage the substrate (dark) is exposed between the particles. The percent coverage of nanoparticles on the surfaces of the R30 and R50 films is plotted as a function of time and nanoparticle suspension concentration, as seen in Figure 3. There are three distinct regions in the reaction kinetics in all four sets of data. The first is an induction period, where the percent coverage of nanoparticles on the polymer substrates remains nearly constant with time. The duration of this induction period decreases as both the surface concentration of acrylic acid groups and nanoparticle suspension concentration increase. In the second region, the percent coverage of nanoparticles on the

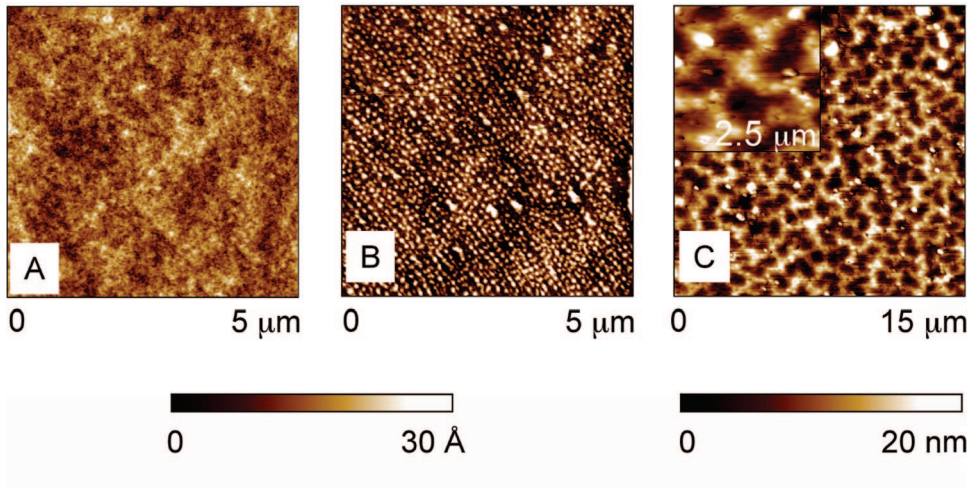

Figure 4. AFM images of the R50 copolymer film: (A) after annealing at 185 °C for 15 h (5 μm × 5 μm, Δz = 30 Å); (B) in situ after 2 h in pH 8 buffer (5 μm × 5 μm, Δz = 30 Å); (C) in situ, after 2 h in pH 8 buffer, 1 h in water, and 1.5 h in ethanol (15 μm × 15 μm, Δz = 20 nm). Inset in (C) is a 2.5 μm × 2.5 μm image of the R50 honeycomb morphology that develops in ethanol and shows that the honeycomb cells are composed of the smaller acrylic acid protrusions seen in (B) (Δz = 20 nm).

polymer substrates increases sharply with time. In the third region, the percent coverage of nanoparticles levels off, with little to no increase with increasing time. The origins of these three regions will be described in detail in section 4.

2. Surface Characterization of Swollen P(S-*ran*-AA) Films. In-situ AFM was used to interrogate the morphological changes on the surface of the P(S-*ran*-AA) films under the same conditions as the nanoparticle coupling reaction. This was performed to understand the surface environment the nanoparticles encountered during attachment. Figure 4 shows these morphological changes for the R50 film. The films were imaged first in air under ambient conditions (Figure 4A), where the dry film exhibits a featureless surface with a roughness around 9 Å. A pH 8 phosphate buffer was then introduced into the liquid cell sample holder. Within 30 min, protrusions about 2.5−3 nm in height began to swell from the surface of the polymer films. These protrusions, considered to be regions of acrylic acid enrichment, retained the same dimensions for the remainder of the 2 h buffer treatment (Figure 4B). Swollen acrylic acid domains show some alignment in the AFM image in Figure 4B as well as images from other samples. This is most likely due to spin-coating and a topic for future investigation. The protrusions composed about 19 ± 4% and 10 ± 3% of the surfaces of the R50 and R30 polymers, respectively. The polymer surface was then imaged in DIUF water for 1 h, simulating the conditions for activating the acrylic acid groups with EDC/NHS. No significant change in the number or dimensions of the protrusions was observed. Finally, the surfaces were imaged in ethanol (Figure 4C), which is the solvent used in the nanoparticle coupling reaction. During ethanol exposure, the protrusions swelled and spread, resulting in an increase in the roughness of the polymer film. The polymer film shows two length scales of roughness: one due to the acrylic acid-rich protrusions (~3 nm in height) observed earlier and one due to the continuous honeycomb morphology (~20 nm in height and 1 μm laterally) resulting from the continued swelling of the films. Although swelling was slower, the R30 polymer films showed similar morphological features as the R50 polymer.

The changes in the surface as monitored by AFM were also characterized using contact angle goniometry. Contact angle measurements were taken after the polymer films were annealed at 185 °C for 15 h, after soaking for 2 h in pH 8 buffer, after 1 h in water, and at various time points after soaking in ethanol. The water contact angle values for the R50 and R30 polymer

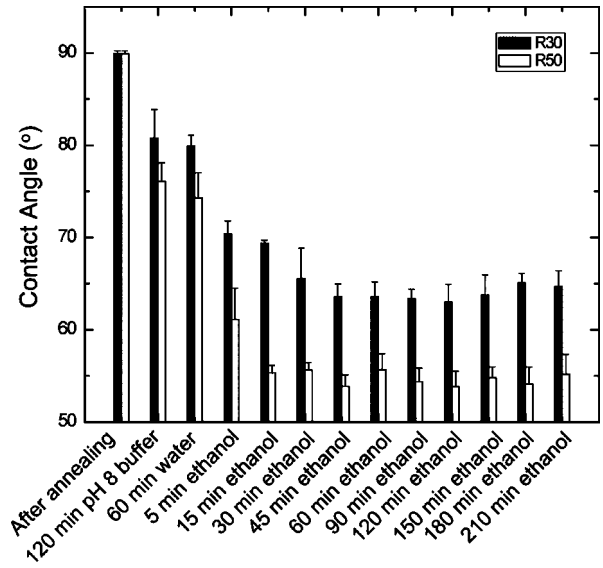

Figure 5. Static contact angles of the R30 (black bars) and R50 (white bars) films after annealing, after 2 h in pH 8 buffer, after 2 h in pH 8 buffer plus 1 h in water, and after 2 h in pH 8 buffer, plus 1 h in water, plus immersion in ethanol (5−210 min).

films as a function of solvent exposure can be seen in Figure 5. After annealing, the contact angle of both the R30 and R50 films was 90°. This is consistent with the contact angle for polystyrene,[38] indicating an enrichment of the hydrophobic styrene at the surface. After immersion in pH 8 buffer, the contact angles of the films were reduced to 80.7 ± 3.1° and 76.1 ± 2.0° for the R30 and R50 polymers, respectively. Taking the contact angle of pure acrylic acid to be 40°,[39] the contact angles of the polymer films after buffer exposure correlate reasonably well with the surface coverage of acrylic acid protrusions calculated from the AFM images using the rule of mixtures (85° and 80° for R30 and R50, respectively). There was no significant change in the contact angle after exposure to water; however, once the films were exposed to ethanol, the contact angles dramatically decreased with time and reached an equilibrium wettability after about 15 min on the R50 polymer and 45 min on the R30 polymer. The equilibrium contact angles for the R30 and R50 polymer films were ~63° and ~55°, respectively. This corresponds to about 55 and 70% surface coverage of acrylic acid in the R30 and R50 polymer

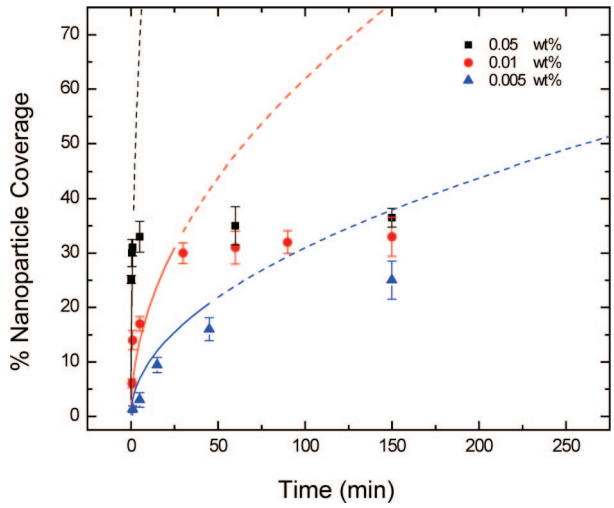

Figure 6. Percent nanoparticle coverage on the SAM surface vs immersion time. Coverage kinetics are shown as a function of particle concentration in solution. All three sets of data [(■) 0.05 wt % particles in solution; (●) 0.01 wt % particles in solution; (▲) 0.005 wt % particles in solution] display $t^{1/2}$ kinetics until saturation is reached at about 30% coverage, as shown by the agreement between the experimental data and the calculated data, solid line (eq 1). The experimental data fall well below the calculated data at long times, dashed line (eq 1); the saturation in the data is due to interparticle repulsions, which decreases the sticking probability of the particles.

films. Although copolymer film surface roughness can change the measured contact angle, in this study the increase in the ratio of rough to smooth surface areas is less than 1%, and therefore this roughness does not significantly change the reported contact angle after exposure to water or ethanol. The enrichment of acrylic acid content at the surfaces of the polymer films was due to the swelling of the acrylic acid protrusions in ethanol, as seen in Figure 4C. This increased swelling of the acrylic acid protrusions is expected because the solubility parameters (δ) of the acrylic acid and ethanol (24.6 and 26 $MPa^{1/2}$, respectively) are very similar, making ethanol a much better solvent for the acrylic acid than water ($\delta = 47.9$ $MPa^{1/2}$). None of the solvents to which the polymer films were exposed is a good solvent for polystyrene ($\delta = 17.5$ $MPa^{1/2}$).[38]

The morphological changes in the polymer films upon exposure to solvent, as characterized by AFM and contact angle goniometry, greatly influence the kinetics of the nanoparticle coupling reaction as well as the maximum particle coverage achieved on these surfaces. AFM shows that the surface area of the films increases upon exposure to solvent, while the contact angle data show that the swelling is due to acrylic acid enrichment. The dynamic film surface morphologies and compositions are dependent on the acrylic acid content of the polymer chains. Because the R30 films have a higher styrene content, the swelling of the AA domains at their surfaces is restricted. This is reflected in the increased time required for the R30 films to achieve an equilibrium contact angle and surface morphology (i.e., an equilibrium surface composition), relative to the R50 films. This effect of the morphology evolution will be discussed in section 4.

3. Kinetics of Nanoparticle Coupling to SAM. To understand why the nanoparticle coverage kinetics on the P(S-*ran*-AA) surfaces showed a unique, three-stage pattern, a control study was undertaken to observe the kinetics of the nanoparticle coupling reaction on a carboxylic acid-terminated self-assembled monolayer (triethoxysilylpropylsuccinic anhydride). This surface presents a homogeneous monolayer of carboxylic acid groups to the nanoparticles and does not swell during solvent exposure. Figure 6 shows percent coverage of particles on the surface of the SAM versus time at nanoparticle concentrations of 0.05, 0.01, and 0.005 wt %. The percent coverage of particles on the surface increases sharply with time, without the induction period observed in the polymer films. At nanoparticle concentrations of 0.05 and 0.01 wt %, the rapid rise in particle coverage at early time points is followed by a plateau at 30−35% coverage. The data for the 0.005 wt % nanoparticle concentration did not achieve a plateau under the experimental time scale. The kinetics displayed in the SAM system follow a diffusion-limited growth law of $t^{1/2}$ at early time points, while at longer times, interparticle repulsions and spatial limitations result in a plateau in coverage around 30−35%. The nanoparticle coverage (#/length^2), q, can be described at *early* times by the diffusion of spherical particles to a planar surface[40,41]

$$q = 0.707pn(Dt)^{1/2} \quad (1)$$

where p is a sticking probability, n is the concentration of particles in suspension, D is the diffusion coefficient of the nanoparticles, and t is the reaction time. This equation assumes a flux of nanoparticles on a planar surface and includes no adjustable parameters. Initially, because surface coverage is low, repulsion between covalently attached nanoparticles and impinging nanoparticles can be ignored and p can be assumed to equal 1. Using a Stokes−Einstein diffusion coefficient, D, of 20.3 particles/μm^2 for all three particle concentrations, the equations plotted in Figure 6 fit the observed kinetics at early time points. Small variations between the calculated and experimental coverages are expected because eq 1 assumes a monodisperse particle diameter of 15 nm, while the actual particles have a distribution in size. Additionally, at long reaction times for all nanoparticle concentrations, the coverage on the SAMs saturates at about 30−35% (significantly lower than the maximum coverages obtained on the polymer films, 70%). This behavior was also observed by Grabar et al., who attributed the plateaus to a decrease in the sticking probability of the particles caused by a decrease in the number of available binding sites and an increase in interparticle repulsion.[40] The differences in the observed kinetics and maximum particle coverages between the polymer and SAM surfaces will be described in the next section.

4. Kinetic Model of the Nanoparticle Coverage on P(S-*ran*-AA). The particle coverage kinetics on the R30 and R50 films cannot be described using eq 1, which was successfully used to describe particle coverage kinetics on SAM surfaces at early time points. Instead, the film coverage kinetics have three distinct stages: an induction phase, a period with a sharp increase in coverage with time, and a plateau region at maximum coverage for all experimental concentrations of nanoparticles. This three-stage behavior can be understood by considering the P(S-*ran*-AA) surface reconstruction during exposure to the solutions used in nanoparticle attachment. Namely, the nanoparticle coverage depends on the dynamic polymer film surface morphology (characterized by AFM, Figure 4) and the chemical composition of the surface (characterized by contact angle goniometry, Figure 5). A schematic outlining the effects of surface rearrangement on coverage kinetics is illustrated in Figure 7.

After annealing under argon, the P(S-*ran*-AA) films have an enrichment of styrene at the surface of the film (Figure 7A); both R30 and R50 substrates have a postannealing static contact angle of 90°. This is expected because PS has a lower surface energy than PAA. After soaking the films in buffer for 2 h, small, acrylic acid-rich protrusions swell from the surface of the film (Figure 7B). The swollen acrylic acid domains are more mobile and can be activated with NHS (Figure 7C). Contact angle and AFM measurements indicated that the acrylic acid

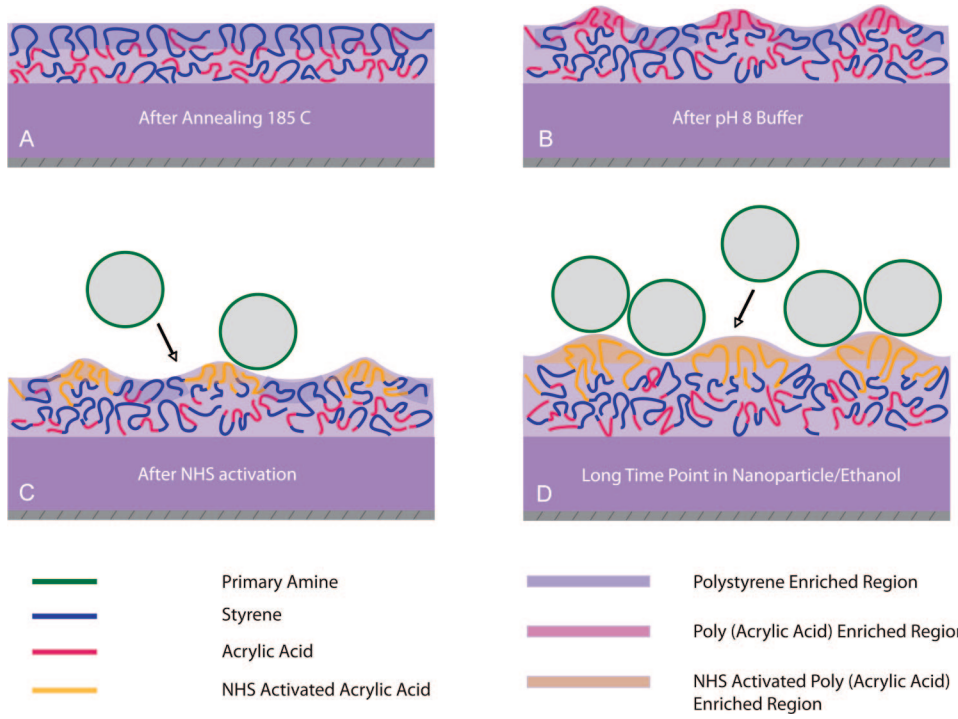

Figure 7. Schematic depicting the effects of surface morphology changes on the observed kinetics for the R30 and R50 polymer films. (A) After annealing the polymer films, there is an enrichment of styrene at the surface because of its lower surface energy. (B) Submersion of the polymer films in pH 8 buffer draws acrylic acid groups to the surface of the films in the form of protrusions about 3 nm tall. (C) The NHS-activated acrylic acid-rich protrusions are not swollen at early time points during ethanol exposure. Because of this, few nanoparticles can react with the film surface. This early morphology is responsible for the induction period. (D) After longer ethanol exposure, the NHS-activated acrylic acid groups swell and spread over the film surface, allowing for rapid reaction with the nanoparticles. The final polymer morphology has a roughness which is similar in size to the nanoparticles. This roughness is responsible for the high particle coverage seen on the polymer, but not on the SAMs. Note: schematic is drawn to scale.

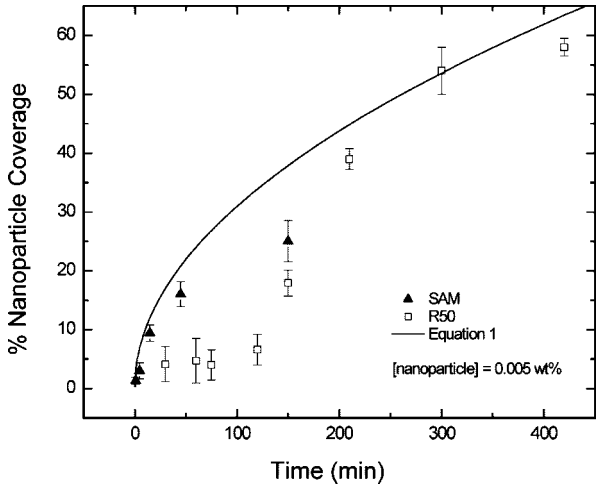

Figure 8. Comparison of the percent nanoparticle coverage vs immersion time for the polymer film (□) and the SAM (▲) at a particle concentration of 0.005 wt %. Diffusion-limited attachment kinetics (eq 1) are plotted as a solid line. At early time points, the SAM substrate follows diffusion-limited kinetics, until higher coverage results in interparticle repulsions, causing a plateau in coverage at ~25%. The R50 substrate, however, shows substrate-limited kinetics until ~100 min, at which time the kinetics become diffusion-limited.

content of the surfaces does not change under the activation conditions. When the substrates are exposed to the nanoparticle−ethanol suspensions, the acrylic acid-rich protrusions swell further, increasing the availability of the nanoparticle reaction sites (Figure 7D). At early stages of this swelling, the available reaction sites are more tightly packed, which partly accounts for the observed induction period. Dordi et al. observed a similar induction period for amine coupling to a surface-bound, NHS-activated acrylic acid group and attributed it to steric hindrance in regions of high NHS surface concentration.[42] As the polymer continues to swell during exposure to ethanol, the surface protrusions expand laterally over the film surface, as shown by both AFM imaging (Figure 4) and a decrease in the film contact angle (Figure 5). The increasingly mobile, swollen polymer chains are more available for reaction, resulting in the rapid increase in percent nanoparticle coverage with time. Furthermore, Figure 3 shows that the induction time is found to decrease with nanoparticle concentration. This implies that the polymer surface rearrangement is not solely responsible for the delay in particle attachment.

To test whether the induction period was due to further swelling and mobility of NHS-activated AA groups, the R50 polymer was preswollen before activating the acrylic acid groups and immersing the substrates in the nanoparticle suspensions. By preswelling the polymer films in buffer, water, and then ethanol, the surfaces of the polymer films obtained their acrylic acid-enriched, honeycomb morphology, as seen in Figure 4C. After submerging the preswollen, NHS-activated polymer substrates in both 0.05 and 0.005 wt % nanoparticle suspensions, the induction period disappeared, and $t^{1/2}$ kinetics were observed. Specifically, the R50 substrates reached 70% coverage within the first 10 min after being immersed in the 0.05 wt % nanoparticle suspension and reached 20% coverage within the first 60 min of being immersed in the 0.005 wt % nanoparticle suspension. These values correlate with the expected coverages calculated by eq 1 under the experimental conditions. These control experiments demonstrate that the induction period is due to rearrangement of the polymeric acrylic acid groups in the reaction solvent.

For the highest particle concentration (0.05 wt %), the coverage reached a plateau at about 70% coverage, equivalent to a random close-packed monolayer on a planar surface. This plateau is purely due to a physical constraint; i.e., no space is available for an incoming particle to fit between already-attached particles and react with the surface of the polymer. At 0.005 wt %, however, the plateau in nanoparticle coverage occurred before a full monolayer of particles was achieved because of the slower kinetics relative to the 0.05 wt % case. Figure 8 illustrates the differences in the coverage kinetics on the SAM and polymer surfaces. Diffusion-limited coverage kinetics described by eq 1 are shown as a solid line. At early time points, the SAM surface coverage follows diffusion-limited kinetics and then plateaus at ∼25% coverage, due to interparticle repulsions. The R50 substrate shows an induction period, during which the kinetics are substrate limited. After ∼100 min, the induction period ends and the coverage becomes diffusion limited, as described by eq 1. Small discrepancies between the R50 values and eq 1 line are expected because of the previously described polydispersity in the particle diameters. The disparity in the attainable coverages on the SAMs and the polymer surfaces can be attributed to the swelling of the polymers in ethanol, which increases the roughness and surface area of the films. The roughened surface provides greater area for the nanoparticles to attach to the polymer. Additionally, the polymer swelling must offset the interparticle repulsions that cause the plateau in particle coverage at 35% in the SAMs.

Conclusion

In summary, we present a novel approach to prepare nanoparticle assemblies covalently bonded to random copolymer films and SAMs. The surface coverage was found to depend on the concentrations of nanoparticles in suspension, acrylic acid functionalities at the substrate surface, and reaction time. In addition, the effects of polymer surface rearrangement on particle coverage were explored by AFM and contact angle goniometry. Surface enrichment of acrylic acid and film swelling under the nanoparticle coupling conditions was found to be responsible for dramatically increasing the maximum particle coverage on the polymer films to approximately twice the coverage attainable on SAM substrates. These novel materials provide a unique platform for studies requiring surfaces with controlled densities of discrete nanoparticles. These surfaces would be particularly useful for studying cell adhesion because the nanoparticles could be functionalized with cell binding peptides, and then the particle density could be varied to give necessary insights into cellular mechanics.

Acknowledgment. This research is supported in part by National Science Foundation (NSF) CAREER award (DMR-0548070) (S.Y., M.D.M.) and NSF/Polymer Program (DMR02-34903), NSF/MRSEC (DMR05-20020), and NSF/NSEC (DMR04-25780) (R.J.C., M.D.M.). M.D.M. acknowledges partial support from the Aston Fellowship (UPenn) and the Pennsylvania Muscle Institute (UPenn) for a seed grant.

References and Notes

(1) Shipway, A. N.; Katz, E.; Willner, I. *ChemPhysChem* **2000**, *1*, 18–52.
(2) Tsai, H.-J.; Lee, Y.-L. *Langmuir* **2007**, *23*, 12687–12692.
(3) Tsai, P.-S.; Yang, Y.-M.; Lee, Y.-L. *Langmuir* **2006**, *22*, 5660–5665.
(4) Ming, W.; Wu, D.; van Benthem, R.; de With, G. *Nano Lett.* **2005**, *5*, 2298–2301.
(5) Cebeci, F. C.; Wu, Z.; Zhai, L.; Cohen, R. E.; Rubner, M. F. *Langmuir* **2006**, *22*, 2856–2862.
(6) Musick, M. D.; Keating, C. D.; Keefe, M. H.; Natan, M. J. *Chem. Mater.* **1997**, *9*, 1499–1501.
(7) Boettcher, S. W.; Strandwitz, N. C.; Schierhorn, M.; Lock, N.; Lonergan, M. C.; Stucky, G. D. *Nat. Mater.* **2007**, *6*, 592–596.
(8) Musick, M. D.; Keating, C. D.; Lyon, A.; Botsko, S. L.; Pena, D. J.; Hooliway, W. D.; McEvoy, T. M.; Richardson, J. N.; Natan, M. J. *Chem. Mater.* **2000**, *12*, 2869–2881.
(9) Kim, J. Y.; Osterloh, F. E. *J. Am. Chem. Soc.* **2006**, *128*, 3868–3869.
(10) Tokareva, I.; Minko, S.; Fendler, J. H.; Hutter, E. *J. Am. Chem. Soc.* **2004**, *126*, 15950–15951.
(11) Phely-Bobin, T. S.; Muisener, R. J.; Koberstein, J. T.; Papadimitrakopoulostrast, F. *Adv. Mater.* **2000**, *12*, 1257–1261.
(12) Darling, S. B.; Yufa, N. A.; Cisse, A. L.; Bader, S. D.; Sibener, S. J. *Adv. Mater.* **2005**, *17*, 2446–2450.
(13) Sun, S.; Anders, S.; Hamann, H. F.; Thiele, J.-U.; Baglin, J. E. E.; Thomson, T.; Fullerton, E. E.; Murray, C. B.; Terris, B. D. *J. Am. Chem. Soc.* **2002**, *124*, 2884–2885.
(14) Baron, R.; Huang, C.-H.; Bassani, D. M.; Onopriyenko, A.; Zayats, M.; Willner, I. *Angew. Chem.* **2005**, *117*, 4078–4083.
(15) Lee, S. W.; Drwiega, J.; Wu, C. W.; Mazyck, D.; Sigmund, W. M. *Chem. Mater.* **2004**, *16*, 1160–1164.
(16) Zhong, Z.; Lin, J.; Teh, S.-P.; Teo, J.; Dautzenberg, F. M. *Adv. Funct. Mater.* **2007**, *17*, 1402–1408.
(17) Walter, N.; Selhuber, C.; Kessler, H.; Spatz, J. *Nano Lett.* **2006**, *6*, 398–402.
(18) Blummel, J.; Perschmann, N.; Aydin, D.; Drinjakovic, J.; Surrey, T.; Lopez-Garcia, M.; Kessler, H.; Spatz, J. P. *Biomaterials* **2007**, *28*, 4739–4747.
(19) Bhat, R. R.; Genzer, J. *Nanotechnology* **2007**, *18*, 1–6.
(20) Bhat, R. R.; Fischer, D. A.; Genzer, J. *Langmuir* **2002**, *18*, 5640–5643.
(21) Lee, D.; Gemici, Z.; Rubner, M. F.; Cohen, R. E. *Langmuir* **2007**, *23*, 8833–8837.
(22) Lee, D.; Rubner, M. F.; Cohen, R. E. *Nano Lett.* **2006**, *6*, 2305–2312.
(23) Smoukov, S. K.; Bishop, K. J. M.; Kowalczyk, B.; Kalsin, A. M.; Grzybowski, B. A. *J. Am. Chem. Soc.* **2007**, *129*, 15623–15630.
(24) Glass, R.; Moller, M.; Spatz, J. *Nanotechnology* **2003**, *14*, 1153–1160.
(25) Kastle, G.; Boyen, H.-G.; Weigl, F.; Lengl, G.; Herzog, T.; Ziemann, P.; Riethmuller, S.; Mayer, O.; Hartmann, C.; Spatz, J. P.; Moller, M.; Ozawa, M.; Banhart, F.; Garnier, M. G.; Oelhafen, P. *Adv. Funct. Mater.* **2003**, *13*, 853–861.
(26) Grabar, K. C.; Griffith Freeman, R.; Hommer, M. B.; Natan, M. *J. Anal. Chem.* **1995**, *67*, 735–743.
(27) Zou, S.; Hong, R.; Emrick, T.; Walker, G. C. *Langmuir* **2007**, *23*, 1612–1614.
(28) Binder, W. H.; Kluger, C.; Straif, C. J.; Friedbacher, G. *Macromolecules* **2005**, *38*, 9405–9410.
(29) Haryono, A.; Binder, W. H. *Small* **2006**, *2*, 600–611.
(30) Binder, W. H.; Kluger, C.; Josipovic, M.; Straif, C. J.; Friedbacher, G. *Macromolecules* **2006**, *39*, 8092–8101.
(31) Li, B.; Li, C. Y. *J. Am. Chem. Soc.* **2007**, *129*, 12–13.
(32) Bhat, R. R.; Genzer, J.; Chaney, B. N.; Sugg, H. W.; Liebmann-Vinson, A. *Nanotechnology* **2003**, *14*, 1145–1152.
(33) Schmitt, J.; Decher, G.; Dressick, W. J.; Brandow, S. L.; Geer, R. E.; Shashidhar, R.; Calvert, J. M. *Adv. Mater.* **1997**, *9*, 61–65.
(34) Russell, L. E.; Galyean, A. A.; Notte, S. M.; Leopold, M. C. *Langmuir* **2007**, *23*, 7466–7471.
(35) Lee, M. H.; Brass, D. A.; Morris, R.; Composto, R. J.; Ducheyne, P. *Biomaterials* **2005**, *26*, 1721–1730.
(36) Lee, M. H.; Boettiger, D.; Ducheyne, P.; Composto, R. J. *Silanes and Other Coupling Agents* **2007**, *4*, 1–16.
(37) Plummer, S. T.; Bohn, P. W. *Langmuir* **2002**, *18*, 4142–4149.
(38) Brandrup, J.; Immergut, E. H. *Polymer Handbook*, 3rd ed.; John Wiley & Sons: New York, 1989.
(39) Julthongpiput, D.; Lin, Y.-H.; Teng, J.; Zubarev, E. R.; Tsukruk, V. V. *J. Am. Chem. Soc.* **2003**, *125*, 15912–15921.
(40) Grabar, K. C.; Smith, P. C.; Musick, M. D.; Davis, J. A.; Walter, D. G.; Jackson, M. A.; Guthrie, A. P.; Natan, M. J. *J. Am. Chem. Soc.* **1996**, *118*, 1148–1153.
(41) Hayat, M. A. *Colloidal Gold: Principles, Methods, and Applications*; Academic Press: San Diego, 1989; Vol. *1*, p 536.
(42) Dordi, B.; Pickering, J. P.; Schonherr, H.; Vancso, G. J. *Surf. Sci.* **2004**, *570*, 57–66.

MA8023156